Article

Kinetic Discrimination of Sequence-Specific DNA–Drug Binding Measured by Surface Plasmon Resonance Imaging and Comparison to Solution-Phase Measurements

Lauren K. Wolf, Yang Gao, and Rosina M. Georgiadis

J. Am. Chem. Soc., **2007**, 129 (34), 10503-10511• DOI: 10.1021/ja072401l • Publication Date (Web): 08 August 2007

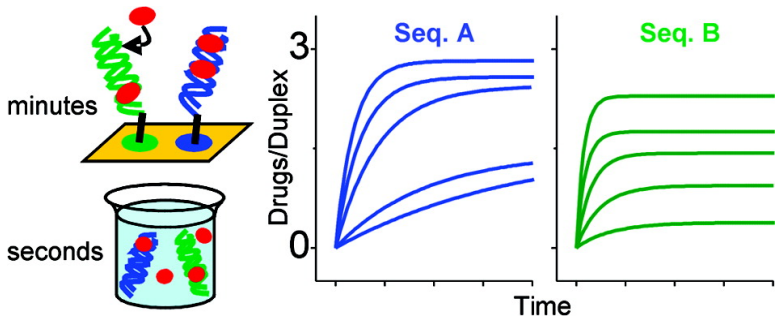

More About This Article

Additional resources and features associated with this article are available within the HTML version:

- Supporting Information
- Links to the 6 articles that cite this article, as of the time of this article download
- Access to high resolution figures
- Links to articles and content related to this article
- Copyright permission to reproduce figures and/or text from this article

View the Full Text HTML

J|A|C|S
ARTICLES
Published on Web 08/08/2007

Kinetic Discrimination of Sequence-Specific DNA−Drug Binding Measured by Surface Plasmon Resonance Imaging and Comparison to Solution-Phase Measurements

Lauren K. Wolf, Yang Gao, and Rosina M. Georgiadis*

Contribution from the Department of Chemistry, Metcalf Center for Science and Engineering, Boston University, 590 Commonwealth Avenue, Boston, Massachusetts 02215

Received April 5, 2007; E-mail: rgeorgia@bu.edu

Abstract: We demonstrate the use of surface plasmon resonance (SPR) imaging for direct detection of small-molecule binding to surface-bound DNA probes. Using a carefully designed array surface, we quantitatively discriminate between the interactions of a model drug with different immobilized DNA binding sites. Specifically, we measure the association and dissociation intercalation rates of actinomycin-D (ACTD) to and from double-stranded 5′-TGCT-3′ and 5′-GGCA-3′ binding sites. The rates measured provide mechanistic information about the DNA−ACTD interaction; ACTD initially binds nonspecifically to DNA but exerts its activity by dissociating slowly from strong affinity sites. We observe a slow dissociation time of $k_d^{-1} = 3300 \pm 100$ s for ACTD bound to the strong affinity site 5′-TGCT-3′ and a much faster dissociation time (210 ± 15 s) for ACTD bound weakly to the site 5′-GGCA-3′. These dissociation rates, which differ by an order of magnitude, determine the binding affinity for each site (8.8×10^6 and 1.0×10^6 M^{-1}, respectively). We assess the effect the surface environment has on these biosensor measurements by determining kinetic and thermodynamic constants for the same DNA−ACTD interactions in solution. The surface suppresses binding affinities ∼4-fold for both binding sites. This suppression suggests a barrier to DNA−drug association; ACTD binding to duplex DNA is ∼100 times slower on the surface than in solution.

Introduction

Analytical screening methods that can rapidly identify strong-affinity drug compounds and their binding mechanisms are in high demand. Drugs that bind in a sequence-specific manner to DNA, thereby inhibiting gene expression, are of particular interest. Actinomycin-D is one such molecule that has been widely studied both in solution and, more recently, at surfaces. Current techniques for identifying drug binding sites and their affinities, such as DNA footprinting, require labels and long digestion/purification times.[1] Other more high-throughput assays, such as fluorescent intercalator displacement (FID), provide no kinetic (mechanistic) information and are limited to measuring affinities greater than that of the competitive intercalator.[2,3] Surface-based optical biosensors, however, are capable of rapid, label-free, in situ kinetic and thermodynamic measurements; however, these refractive-index-based methods have not been widely used for the direct detection of low-molecular-weight compounds because of limited sensitivity. We have recently shown that surface plasmon resonance (SPR) imaging can achieve sufficient sensitivity to detect DNA−drug interactions.[4]

Past attempts to use SPR spectroscopy for directly monitoring kinetics as well as thermodynamics of DNA−drug binding have been limited. Results are difficult to interpret because of the refractive index amplification schemes employed to improve detection. Long biological DNA probes containing many different binding sites lead to higher signal levels but, for sequence-specific drug molecules, yield measured binding affinity and rate constants that are averages from all binding sites involved.[5] Researchers have used shorter DNA probes linked to three-dimensional dextran gels to achieve a higher density of drug binding sites per unit sensor surface area and, thus, higher SPR signal as well.[6,7] However, significant non-specific binding to the sensor surface and potential mass-transport-limited diffusion within the gel[8] can interfere with kinetic and thermodynamic analysis.[9]

To eliminate these complications and demonstrate the application of optical biosensing to direct multiplexed drug screening, we have carefully designed an array surface for studying the binding of a model sequence-specific drug molecule by SPR imaging. The surface blocks nonspecific drug binding and contains a single type of binding site per DNA array probe spot to ensure acquisition of site-specific kinetic and thermodynamic constants. Each 25-mer DNA probe studied contains three non-interacting, identical binding sites. Tripling the number

(1) Shubsda, M.; Kishikawa, H.; Goodisman, J.; Dabrowiak, J. *J. Mol. Recognit.* **1994**, *7*, 133−139.
(2) Tse, W. C.; Boger, D. L. *Acc. Chem. Res.* **2004**, *37*, 61−69.
(3) Lewis, M. A.; Long, E. C. *Bioorg. Med. Chem.* **2006**, *14*, 3481−3490.
(4) Cooper, M. A. *Nat. Rev. Drug Discovery* **2002**, *1*, 515−528.
(5) Tombelli, S.; Minunni, M.; Mascini, M. *Anal. Lett.* **2002**, *35*, 599−613.
(6) Ciolkowski, M. L.; Fang, M. M.; Lund, M. E. *J. Pharm. Biomed. Anal.* **2000**, *22*, 1037−1045.
(7) Bischoff, G.; Bischoff, R.; Birch-Hirschfeld, E.; Gromann, U.; Lindau, S.; Meister, W.-V.; Bambirra, S. d. A.; Bohley, C.; Hoffmann, S. *J. Biomol. Struct. Dyn.* **1998**, *16*, 187−202.
(8) Myszka, D. G.; He, X.; Dembo, M.; Morton, T. A.; Goldstein, B. *Biophys. J.* **1998**, *75*, 583−594.
(9) Ober, R. J.; Ward, E. S. *Anal. Biochem.* **1999**, *271*, 70−80.

of binding sites serves to maximize SPR signal for experiments performed on the relatively low-density (submonolayer) duplex films in each addressable array spot. Using careful control experiments and angle-resolved imaging,[10] we quantify the number of drug molecules binding to each type of site for all patterned spots on the sensor surface. We also simultaneously measure the rates of drug binding to multiple spots and find that DNA−drug molecule interaction is kinetically and thermodynamically distinct for each binding site. In fact, the binding site dependence for the two surface-bound duplexes studied closely matches the behavior reported for the same binding sites in solution.[11]

These proof-of-concept studies employ the model anticancer drug, actinomycin-D (ACTD). ACTD has been the subject of intense solution-phase study since the time of its isolation from the bacterium species *Streptomyces* and the subsequent discovery of its anti-tumor activity in the early 1940s. It is believed that ACTD binds to DNA with a long residence time, inhibiting gene transcription through the delay of RNA polymerase.[12] The drug's exact DNA-binding mode was widely disputed until the pioneering work of Müller and Crothers in 1968.[13] At that time, it was shown that ACTD intercalated into double-stranded DNA (dsDNA), a mode of DNA binding proposed by Lerman[14] years earlier.

During intercalation, ACTD inserts its planar, phenoxazone ring system between the base pairs of duplex DNA, and its pentapeptide rings interact with the minor groove. Unlike other ubiquitous intercalators, such as ethidium bromide, ACTD displays a preference for inserting itself between 5′-dGpdC-3′ base pairs. Sobell and co-workers used X-ray crystallography to show that this specificity was mainly caused by the pentapeptide features of ACTD.[15] Specifically, strong hydrogen bonds connect the guanine 2-amino groups of the DNA with the carbonyl oxygens of the drug L-threonine residues. No such strong bonding to other DNA bases occurs; consequently, ACTD does not specifically bind to tracts of dA or dT.[16]

The effects of the ACTD peptide rings extend farther than just the phenoxazone insertion site. The flanking sequences adjacent to the site (5′-XGCY-3′, where X and Y = T, G, C, or A) are also profoundly important to DNA−drug complex formation. Chen illustrated this dependence through a number of systematic solution-phase studies on the interaction of short, single-binding-site-containing duplexes with ACTD.[11,17] Using 10-mers of sequence d(ATA-XGCY-ATA)-d(TAT-Y′GCX′-TAT), where X and Y are complementary to X′ and Y′, respectively, Chen found that ACTD binding affinity could vary by more than an order of magnitude, depending on the identity of the flanking base pairs. This flanking sequence dependence was later explained by crystallography and molecular modeling studies.[18] The minor groove shape at the binding site is affected by the flanking base pairs and accommodates pentapeptide residues differently. In particular, the ability of the isopropyl group on the *N*-methyl-L-valine residue to fit into the groove controls the strength of ACTD binding.[18,19]

Table 1. Oligonucleotide Sequences and Binding Sites

oligonucleotide	sequence[a]
P_s	5′-TTTTGCTAATATGCTATAATGCTAT-3′
T_s	3′-AAAACGATTATACGATATTACGATA-5′
P_w	5′-TTAGGCATTTAGGCATATTGGCATT-3′
T_w	3′-AATCCGTAAATCCGTATAACCGTAA-5′
poly(dT)	5′-$(T)_{25}$-3′

[a] Binding sites are underlined.

We observe similar discrimination between binding sites with our surface-based imaging measurements. Although the surface binding affinities we measure for individual binding sites (with different flanking base pairs) agree with those determined by Chen for short duplexes in solution,[11] we find a ∼4-fold suppression in binding affinities on the surface when directly compared to the results obtained for our longer sequences in solution. The surface environment most likely affects the DNA−drug interaction by sterically hindering ACTD binding within the immobilized DNA film; we observe drug adsorption rates 100 times faster in solution than on the surface. This direct solution/surface comparison allows the prediction of solution-phase (or in vivo) binding behavior from surface-based biosensor measurements for similar systems.

Materials and Methods

Sequence Selection and Handling. The probe (P) and target (T) duplex pairs, listed in Table 1, were designed to have three ACTD binding sites. The binding sites are equivalently spaced in the drug-binding duplexes studied; the spacer dA and dT nucleotide sequences between sites vary to prevent target DNA cross-hybridization (discussed below). Adjacent binding sites are spaced at least four base pairs apart to prevent inhibition of drug binding by neighbor exclusion. Although binding cooperativity of ACTD has been shown for biological DNA containing many different binding sites in the past,[20] we find no measurable cooperativity for our 25-mer sequences; the three identical binding sites appear to have the same association and dissociation rate constants (and, thus, equilibrium constants) within the error of our measurements (see Supporting Information, Figure S1).

The specific binding sites contained within the P_sT_s and P_wT_w duplexes were selected on the basis of previous affinity measurements for single binding sites in short 10-mer duplexes in solution.[11] Specifically, the duplex P_sT_s contains the 5′-TGCT-3′/3′-ACGA-5′ site found to have a relatively strong solution-phase literature ACTD binding affinity (6.7×10^6 M^{-1}), while the duplex P_wT_w contains the 5′-GGCA-3′/3′-CCGT-5′ site of weaker affinity (2.1×10^6 M^{-1}). Poly(dT) is a control sequence to which ACTD should not bind.

All oligonucleotides were purchased from Integrated DNA Technologies (IDT, Coralville, IA). All polyacrylamide gel electrophoresis-purified target DNA sequences were used as received. The high-performance liquid chromatography-purified 5′ thiol-terminated (HS-$(CH_2)_6$-) sequences, however, were received protected by a disulfide mercaptohexanol group. This group was cleaved from the oligonucleotides by treatment with 0.04 M dithiothreitol in 0.17 M phosphate buffer (pH 8.0) at room temperature for at least 16 h. The cleaved products were separated on a size-exclusion NAP-10 column (Amersham Biosciences, Piscataway, NJ), equilibrated with 0.01 M sodium phosphate buffer (pH 6.8). The thiolated single-strand eluent was tested with UV absorbance spectroscopy (Cary 100 Bio, Varian Inc., Palo

(10) Wolf, L. K.; Fullenkamp, D. E.; Georgiadis, R. M. *J. Am. Chem. Soc.* **2005**, *127*, 17453−17459.
(11) Chen, F. M. *Biochemistry* **1992**, *31*, 6223−6228.
(12) White, R. J.; Phillips, D. R. *Biochemistry* **1988**, *27*, 9122−9132.
(13) Müller, W.; Crothers, D. M. *J. Mol. Biol.* **1968**, *35*, 251−290.
(14) Lerman, L. S. *J. Mol. Biol.* **1961**, *3*, 18−30.
(15) Jain, S. C.; Sobell, H. M. *J. Mol. Biol.* **1972**, *68*, 1−20.
(16) Ren, J.; Chaires, J. B. *Biochemistry* **1999**, *38*, 16067−16075.
(17) Chen, F. M. *Biochemistry* **1988**, *27*, 6393−6397.
(18) Kamitori, S.; Takusagawa, F. *J. Am. Chem. Soc.* **1994**, *116*, 4154−4165.
(19) Takusagawa, F.; Wen, L.; Chu, W.; Li, Q.; Takusagawa, K. T.; Carlson, R. G.; Weaver, R. F. *Biochemistry* **1996**, *35*, 13240−13249.
(20) Winkle, S. A.; Krugh, T. R. *Nucleic Acids Res.* **1981**, *9*, 3175−3186.

Alto, CA) at 260 nm to establish concentration for further preparation and immediate immobilization.

Chemicals. ACTD from Sigma was dissolved in methanol (Aldrich, spectrophotometric grade) before use. The concentration of ACTD was determined using an extinction coefficient of 24 500 M^{-1} cm^{-1} at 440 nm.[21] Mercaptoundecanoic acid (MUA, Aldrich) surface back-filling and full monolayer formation were carried out in ethanol (Aldrich, ACS grade). DNA target hybridizations were carried out in 1 M NaCl/TE (TE = 10 mM Tris, 1 mM EDTA, pH ~7.6) buffer solution, while drug binding and solution-phase kinetic measurements were carried out in 0.1 M NaCl/TE. All salts were obtained from Sigma (SigmaUltra grade) and dissolved in 18 MΩ·cm distilled water. Sodium dodecyl sulfate (SDS, Sigma-Aldrich) was used for surface regeneration (0.4% by weight) and solution-phase dissociation (1%) measurements.

Duplex Stability Measurements. We characterized the solution-phase melting temperature (T_m) of each duplex by melting the probe–target pairs in the absence of ACTD and measuring the changes in UV absorbance at 260 nm with a Varian Cary 100 instrument (Peltier thermostatable multicell holder with temperature accuracy $<\pm 0.3$ °C). Because DNA-intercalating compounds such as ACTD stabilize duplex DNA upon binding,[22] we also measured the change in duplex melting temperature (ΔT_m) in the presence of intercalator. Values of T_m and ΔT_m can be found in Table S1 (Supporting Information), along with details of measurements and analysis. P_sT_s is stabilized by ACTD more than P_wT_w (larger ΔT_m), indicating stronger P_sT_s drug–molecule binding affinity.

Drug Binding to Multi-probe Films with Drug-Resistant Backgrounds. We have shown previously that monolayer films of MUA are resistant to nonspecific ACTD surface binding.[10] For the surface drug-binding studies presented here, we hand-spotted thiol-terminated DNA onto a bare gold surface and back-filled with MUA. Back-filling with MUA blocks nonspecific drug binding, just as back-filling with mercaptohexanol has prevented nonspecific DNA target binding to the surface during DNA hybridization studies in the past.[23] No binding of target DNA or ACTD was observed on control poly(dT) spots patterned by this method (see Supporting Information, Figure S2).

By hand-spotting 2 μM solutions (0.5 M NaCl) of 5′ thiol-terminated P_s, P_w, and poly(dT) onto a bare gold-coated glass slide for 1.5–2 h, we obtained average ssDNA densities of $(4.8 \pm 0.2) \times 10^{12}$, $(4.9 \pm 1.3) \times 10^{12}$, and $(1.4 \pm 0.3) \times 10^{13}$ molecules/cm^2, respectively. The densities for this array surface (Drug Array 1, Figure 1A) were characterized by angle-resolved SPR imaging[10] and calculated from the average of two regions of interest (ROIs) in two different hand spots for each probe sequence. Probe density is evaluated by fitting angle-resolved SPR imaging curves, such as those shown in Figure 1B, to Fresnel optical models (see below for details). Despite identical thiol exposure times, the density of immobilized poly(dT) (labeled "C" for control in Figure 1A) on the surface is greater than that obtained for either P_s or P_w; poly(dT) contains only dT nucleotides, which bind weakly to gold and hinder the thiol immobilization process less than other nucleotides.[24]

Prior to hand-spotting (0.4 μL), the gold-coated glass slide (SF-10 glass, 18 × 18 mm^2, GenTel BioSciences, Inc., Madison, WI) was piranha-cleaned (7:3 H_2SO_4:H_2O_2 (30% solution) at >50 °C) for 5 min, rinsed with copious amounts of water, and dried under nitrogen. After 2 h in a humidity chamber following spotting, the slide was soaked in ~1.5 M NaCl, rinsed with water, dried under nitrogen, and immersed in a 2 mM solution of MUA in ethanol for 6 h. The slide was then rinsed with ethanol and hot water (~65 °C for 10 min), dried, and immersed again in MUA for 2 h before rinsing and imaging.

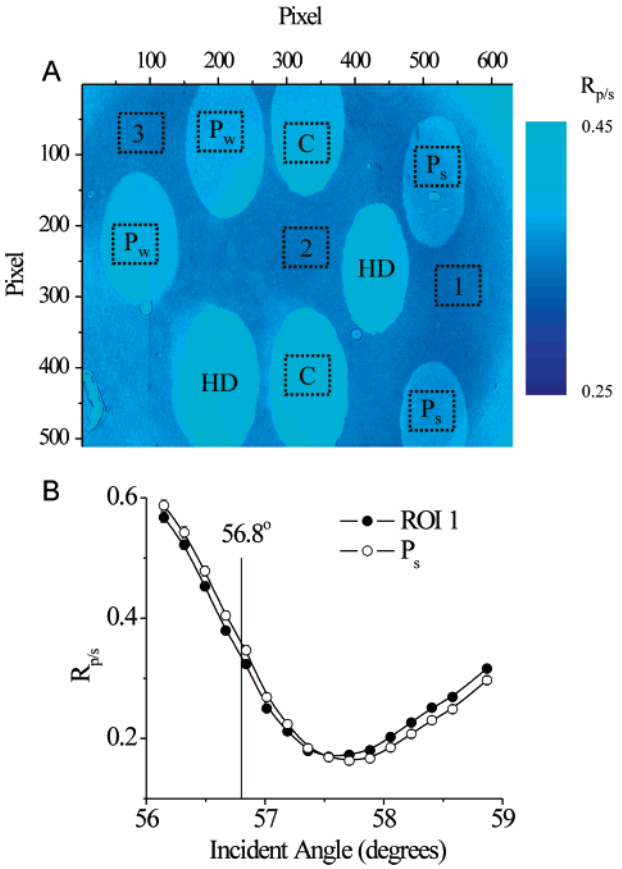

Figure 1. (A) Image of surface (Drug Array 1) fabricated by immobilization of thiolated DNA probe molecules and used in drug binding studies. Dotted squares indicate the regions of interest (ROIs) monitored during kinetic and angle-resolved measurements. Regions are all approximately 500 × 500 μm^2. A region in each of two probe hand spots for each sequence was monitored (poly(dT) = "C" here). Background MUA regions were also monitored (1–3) and used in angle-resolved analysis to determine DNA densities. The image was acquired at 56.8° in 1 M NaCl/TE. The scratch at the lower left is a scribe mark in the SF-10 slide, while the light area in the upper right-hand corner is caused by the flow cell O-ring. Spots not monitored contain very high probe densities (labeled HD) and are not considered in this work. (B) Example reflectance curves generated by angle-resolved imaging of the fabricated surface. Curves represent the reflectance ratio ($R_{p/s}$) measured in MUA background ROI 1 and the average of both P_s ROIs as a function of incident light angle.

SPR Imaging and Analysis. Development of an SPR imaging instrument for measuring the kinetics and thermodynamics of multiple parallel DNA–drug interactions has been discussed previously.[10] Briefly, the white light from a quartz tungsten halogen source is collimated, filtered (633 nm), p-polarized, and coupled to the gold-coated surface of an SF-10 glass slide through attenuated total reflection. The slide (1 mm thick), sealed to an all-Teflon liquid cell via Kalrez O-ring, is attached to a goniometer-mounted SF-10 equilateral prism by index matching fluid (Cargille Labs, Cedar Grove, NJ, $n = 1.7300$). Reflected light is focused onto a charge-coupled device camera, which is mounted on a rotational arm to accommodate changes in incident light angle. A nematic liquid crystal variable retarder corrects images for variation in the light source by generating s- and p-polarized light via differential applied voltages. P-polarized images are divided by s-polarized images to obtain a corrected image that is spatially normalized for light intensity variations in terms of reflectance ratio, $R_{p/s}$.

We use angle-resolved imaging to directly quantify the number of probe and target molecules immobilizing and binding to our surfaces. This entails varying the incident angle of light entering the prism and collecting p- and s-polarized light images of the surface at each angle. SPR reflectance curves are generated for selected ROIs of the patterned

(21) Chen, F. M. *Biochemistry* **1988**, *27*, 1843–1848.
(22) Bloomfield, V. A.; Crothers, D. M.; Tinoco, I. *Nucleic Acids: Structures, Properties and Functions*; University Science Books: Sausalito, CA, 2000.
(23) Peterlinz, K. A.; Georgiadis, R. M. *J. Am. Chem. Soc.* **1997**, *119*, 3401–3402.
(24) Wolf, L. K.; Gao, Y.; Georgiadis, R. M. *Langmuir* **2004**, *20*, 3357–3361.

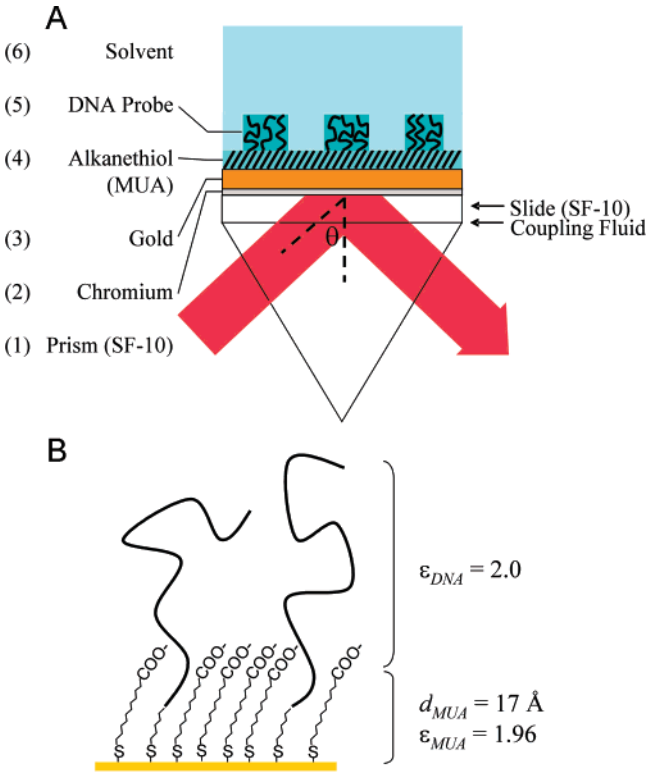

Figure 2. (A) Six-layer configuration for Fresnel modeling of angle-resolved SPR imaging reflectance data obtained from patterned surfaces. The schematic is not drawn to scale; prism and solvent are infinitely thick compared to the chromium adlayer (~10 Å), gold film (~500 Å), alkanethiol layer (17 Å), and probe layer. A thin layer of coupling fluid ($n = 1.7300$) matches the index of the SF-10 glass slide (1 mm thick) and prism, allowing light incidence at the metal interface. (B) Schematic of molecular architecture in thiol-patterned probe spots. The MUA back-fill constitutes most of the diluent layer and is therefore assumed to have the thickness and optical properties of a full MUA monolayer during Fresnel modeling. The DNA probe layer is assumed to have a dielectric constant of 2.0.

array, as illustrated in Figure 1B for hand spots containing probe sequence P_s. The results presented in this work are independent of the specific ROIs chosen; statistical analysis has shown that probe densities and kinetic trends are the same within error whether averaging over the entire hand spot or over smaller (500 × 500 μm^2) regions within the spot. Our analysis neglects regions near spot edges (or rims), where probe densities tend to be very high because of droplet evaporation during fabrication.[25,26]

We characterize the patterned surface by fitting angle-resolved curves to five- and six-layer Fresnel optical models.[27,28] The six possible layers considered in fitting the data are the glass prism, the thin chromium adhesion layer, the gold film, the alkanethiol MUA monolayer, the probe DNA layer, and the solvent, shown in Figure 2A. Each layer has an associated thickness (d) and dielectric constant (ϵ). In order to fit the reflectance curve generated for the MUA background, we use a five-layer model and assume $d_{MUA} = 17$ Å and $\epsilon_{MUA} = 1.96$[29] for characterization of the metal thickness and dielectric constants. Angle-resolved reflectance curves generated for probe DNA spot ROIs are fit to a six-layer model assuming $\epsilon_{DNA} = 2.0$.[24] By combining optical thicknesses and experimentally measured values of refractive index increment (RII) for the DNA adsorbates in the submonolayer, DNA coverage (molecules/cm^2) is calculated, as demonstrated previously.[24] For patterned surfaces fabricated via DNA−thiol immobilization, this analysis assumes that the MUA diluent (back-fill) layer in a probe DNA spot consists mainly of MUA and alkanethiol linker, as shown in Figure 2B. If we consider the theoretical thickness of MUA and the -$(CH_2)_6$- linker, we conclude that only the most proximal two or three DNA base pairs of the 25-mer are expected to be buried in the diluent layer and may be inaccessible to binding.

All SPR imaging kinetic measurements are carried out at a fixed angle; percent changes in reflectance, %ΔR, are monitored over time in selected ROIs for each patterned surface during binding events. The fixed angle chosen to monitor binding kinetics (of DNA or drug) is optimized for each system studied to report the maximum change in reflectance. For example, the image in Figure 1A was taken at 56.8°, as indicated in Figure 1B. This fixed angle provided the greatest contrast for the image and was also used to monitor maximum reflectance changes caused by subsequent DNA target hybridization in the same 1 M NaCl/TE buffer.

DNA hybridization efficiencies are calculated on the basis of the relationship between changes in reflectance and refractive index (%ΔR vs Δn) determined previously for our molecular architecture and instrument.[10] Values of %ΔR are measured at the angle of maximum reflectance for the probe spot and background before and after DNA target hybridization. These values are converted into Δn on the basis of our %ΔR vs Δn relationship and divided ($\Delta n_{target}/\Delta n_{probe}$) to yield efficiency. For all hybridizations carried out during the drug kinetic measurements presented in this work, efficiencies of 42 ± 5% and 41 ± 6% were attained on the similar density P_s (4.8×10^{12} molecules/cm^2) and P_w (4.9×10^{12} molecules/cm^2) spots studied, respectively.

The number of drug molecules bound to the surface (per duplex) is also calculated from values of Δn, as discussed previously.[10] We can determine the number of drug molecules bound per duplex by comparing the refractive index changes determined for each drug binding event to Δn for DNA hybridization, respectively.[30] For this calculation to be valid, we consider and correct for differences in both the molecular weight and refractive index increment (dn/dc) of target DNA and ACTD. Consideration of the difference in RII for DNA and drug is especially important; without accounting for the difference (~0.19 for DNA targets and 0.256 for ACTD measured previously[10,24]), overestimation of drug molecules bound per duplex occurs (33% overestimation here). This may partially explain a previous report of six or seven ACTD molecules binding to a 47-mer containing only four 5′-GC-3′ binding sites.[6] The difference in RII for ACTD and duplex was not considered in quantitative analysis in that study.

Surface Drug Binding and Analysis. Sequential ACTD binding experiments at different concentrations are carried out on duplex films patterned onto the surface (Drug Array 1, Figure 1A). For each drug concentration studied, the duplex surface is first prepared by target hybridization. After ACTD association and dissociation are measured, the original probe surface is regenerated by SDS (0.4% by weight). Surface hybridization is achieved with an equimolar mixture of complementary targets (1 μM T_s and T_w in 1 M NaCl/TE). We have shown through control experiments that these targets do not cross-hybridize on the surface; each probe binds only to its complementary target in the presence of the mixture (see Supporting Information, Figure S3). Thereafter, the surface is briefly rinsed with 0.1 M NaCl/TE (no loss of either target is observable within our noise levels on the time scale of the rinse, ~5 min), and ACTD is injected into the static cell (0.3−4 μM in 0.1 M NaCl/TE). After approximately 20 min, the ACTD

(25) Deegan, R. D.; Bakajin, O.; Dupont, T. F.; Huber, G.; Nagel, S. R.; Witten, T. A. *Nature* **1997**, *389*, 827−829.
(26) Bietsch, A.; Hegner, M.; Lang, H. P.; Gerber, C. *Langmuir* **2004**, *20*, 5119−5122.
(27) Peterlinz, K. A.; Georgiadis, R. *Langmuir* **1996**, *12*, 4731−4740.
(28) Georgiadis, R.; Peterlinz, K. P.; Peterson, A. W. *J. Am. Chem. Soc.* **2000**, *122*, 3166−3173.
(29) Jordan, C. E.; Frutos, A. G.; Thiel, A. J.; Corn, R. M. *Anal. Chem.* **1997**, *69*, 4939−4947.

(30) $r = (\Delta n_{ACTD}/\Delta n_{HYB})(RII_{HYB}/RII_{ACTD})(MW_{HYB}/MW_{ACTD})$, where Δn_{ACTD} and Δn_{HYB} are the changes in refractive index determined for ACTD binding and DNA hybridization, respectively. RII_{HYB} and RII_{ACTD} are the refractive index increments of target ssDNA and ACTD measured in our laboratory, and MW_{HYB} and MW_{ACTD} are the molecular weights of target DNA and ACTD (1255.4 g/mol), respectively. r is the resulting number of drug molecules bound per duplex on the surface.

solution is replaced with 0.1 M NaCl/TE buffer and drug dissociation is monitored. Target DNA and any remaining ACTD are removed from the surface by regeneration with SDS.

For the DNA−drug system studied here, additional factors must be considered in the analysis of kinetic imaging data. We correct kinetic binding results for fluctuations in the light source or local refractive index caused by temperature or solution concentration variation by subtracting background ROI responses from probe spot ROI responses monitored over time. The background region should be an area of the surface where no target binding occurs for successful data correction. We have already shown that both MUA alone[10] and MUA back-filled poly(dT) spots block nonspecific drug binding. For the experiments presented here, we have chosen to use the poly(dT) ROIs (control or "C" regions in Figure 1A) to correct the data obtained for drug adsorption and desorption to duplex spots. While these regions are more representative of the DNA probe surface environment experienced by the drug during binding, the choice of poly(dT) as a background over MUA does not appear to affect the drug association and dissociation kinetics measured (see Supporting Information, Figure S4). Slight differences in the $\%\Delta R$ values are observable for the two subtraction methods but are not significant within spot-to-spot variation (typically 8−9%).

Another factor that must be considered in the quantitative analysis of our DNA−drug imaging data is the "nonspecific" binding of ACTD to single-stranded DNA. ACTD has been found to inhibit HIV-1 reverse transcription through ssDNA binding and subsequent blocking of hybridization to acceptor RNA.[31] Further structural studies have shown that ACTD can intercalate into the mismatched bulges and single-stranded loops of metastable DNA hairpins containing guanine bases.[32,33] We do not observe ACTD binding to poly(dT) ssDNA spots, which lack dG nucleotides, but we do observe small amounts of drug binding to both P_s and P_w ssDNA probe spots. Although P_s and P_w were designed to have no inherent secondary structure under our experimental conditions (using the mFold algorithm[34,35]), they appear to form metastable hairpins (or possibly dimers) in the presence of ACTD (see Supporting Information, Figure S5). Because of probe−probe steric and electrostatic hindrance, the arrayed films used in these experiments contain dsDNA and ssDNA components (42 ± 5% P_sT_s duplex and 41 ± 6% for P_wT_w duplex) that can each bind the drug. We account for the small ssDNA contribution to our drug binding measurements through control experiments and find that the observed kinetics are not significantly affected by the correction or ssDNA contribution (see Supporting Information, Figure S6). The ACTD association data presented in this work have been corrected to reflect only drug binding to duplex DNA.

We also correct surface drug dissociation data to account for target DNA loss that accompanies ACTD desorption from P_wT_w films. Although duplex surface films are stable during short buffer rinses, long buffer exposure times cause detectable target de-hybridization, particularly for our P_wT_w films, from which ACTD desorbs rapidly and completely. Because ACTD desorbs much more slowly and incompletely from P_sT_s, correction was not carried out for these films. Figure S7 in the Supporting Information describes correction of ACTD desorption from P_wT_w films by target loss (DNA de-hybridization) simulation.

Solution-Phase Kinetic Measurements. As ACTD binds to duplex DNA, the absorbance band of the drug (λ_{max} = 440 nm) red-shifts, causing a maximal absorbance decrease at 427 nm. The rates of duplex−drug association were, therefore, measured by absorbance spectroscopy at 427 nm in solution. Prior to mixing the duplex and drug, solutions of 5 μM P_sT_s and P_wT_w (in 0.1 M NaCl/TE) were heated rapidly and annealed slowly from 85 to 20 °C at 0.5 °C/min. These solutions were then mixed with equimolar solutions of ACTD (5 μM in 0.1 M NaCl/TE) by syringe injection into an empty quartz cuvette (1 cm path length) equilibrated at 20 °C. Kinetic data were collected continuously during injection, and time zero ($t = 0$) was assigned to the point at which reasonable absorbance values are obtained after injection (the point at which the liquid reaches the instrumental beam height). The final solution volume and DNA−drug complex concentration were 0.3 mL and 2.5 μM, respectively. The validity of this injection method and analysis was determined by monitoring the standard reduction of 2,6-dichlorophenolindophenol (Sigma, ACS reagent) by ascorbic acid (Fisher Scientific) at 524 nm (in 10 mM Tris buffer at pH 7.8). The rate constant obtained for the reduction matched literature results within error[36] (data not shown). Recently, the same injection method was successfully used to investigate the kinetics of solution-phase DNA hybridization (monitoring base pair formation at 260 nm).[37]

Typically, drug dissociation is measured in solution using detergent to induce the process.[38] In order to compare our results to solution-phase literature data, we measure the 1% SDS-induced dissociation of ACTD from our solution-phase duplexes for comparison to literature results. Drug:duplex complexes (1:1, 5 μM in 0.1 M NaCl/TE) were prepared by slow annealing. Equal volumes of drug:duplex and SDS (2% in 0.1 M NaCl/TE) solution were simultaneously injected into an empty cuvette to achieve mixing. Kinetic data were again collected continuously at 427 nm.

Binding site affinities were measured in solution by spectral titration. Using a reverse-titration method,[39,40] a known concentration of each duplex was progressively added to a fixed concentration solution of ACTD (~7 μM in 0.1 M NaCl/TE at 20 °C). The absorbance at 440 nm was monitored. The change in absorbance ($\Delta A_{440\ nm}$) was corrected for dilution and plotted as a function of duplex concentration.

Results and Discussion

Surface Association and Dissociation. As shown in Figure 3, we measured very different drug association behaviors for the hybridized P_sT_s and P_wT_w films. ACTD binds more quickly to P_wT_w than to P_sT_s films but achieves lower saturation levels. At the highest drug concentration explored (4 μM), the P_sT_s film reaches a maximal binding level of ~2.8 drug molecules/duplex, while P_wT_w only reaches ~2.3 drug molecules/duplex. Despite the somewhat dense ($(4.8-4.9) \times 10^{12}$ molecules/cm^2) thiol-immobilized films used in these studies, the drug is still accessing nearly all available surface binding sites (a theoretical maximum of three per duplex). Probe−probe steric crowding does not seem to prevent ACTD from penetrating the brush-like films and eventually binding to sites at the MUA diluent interface.

We are able to kinetically discriminate between the drug binding affinities for the two binding sites (and duplexes) investigated here. The adsorption data presented in Figure 3 were fit with a simplified Langmuir model,

$$\%\Delta R(t) = f_{max}\{1 - e^{-(k_{obs})t}\} \quad (1)$$

(31) Jeeninga, R. E.; Huthoff, H. T.; Gultyaev, A. P.; Berkhout, B. *Nucleic Acids Res.* **1998**, *26*, 5472−5479.
(32) Wegner, G. J.; Wark, A. W.; Lee, H. J.; Codner, E.; Saeki, T.; Fang, S. P.; Corn, R. M. *Anal. Chem.* **2004**, *76*, 5677−5684.
(33) Wadkins, R. M.; Vladu, B.; Tung, C. S. *Biochemistry* **1998**, *37*, 11915−11923.
(34) SantaLucia, J. *Proc. Natl. Acad. Sci. U.S.A.* **1998**, *95*, 1460−1465.
(35) Zuker, M. *Nucleic Acids Res.* **2003**, *31*, 3406−3415.
(36) Tonomura, B.; Nakatani, H.; Ohnishi, M.; Yamaguchi-Ito, J. K. H. *Anal. Biochem.* **1978**, *84*, 370−383.
(37) Gao, Y.; Wolf, L. K.; Georgiadis, R. M. *Nucleic Acids Res.* **2006**, *34*, 3370−3377.
(38) Fox, K. R., Ed. *Drug−DNA Interaction Protocols*; Humana Press: Totowa, NJ, 1997; Vol. 90.
(39) Wadkins, R. M.; Jovin, T. M. *Biochemistry* **1991**, *30*, 9469−9478.
(40) Bailey, S. A.; Graves, D. E.; Rill, R.; Marsch, G. *Biochemistry* **1993**, *32*, 5881−5887.

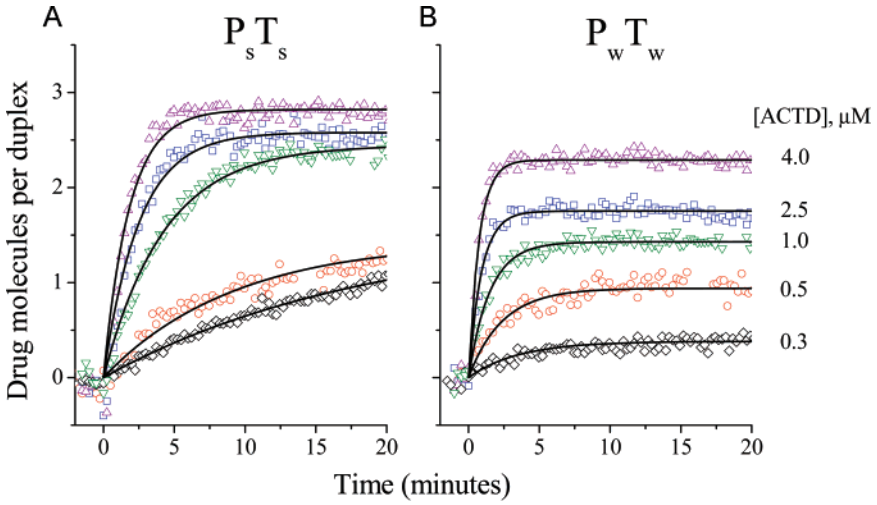

Figure 3. Binding of ACTD to DNA duplex films, P_sT_s (A) and P_wT_w (B), on the same patterned surface at various concentrations (denoted at right). Binding at each concentration is measured for P_sT_s and P_wT_w patterned spots simultaneously. The results shown are the averages of two 50 × 50 pixel ROIs monitored in two different patterned spots of each sequence, indicated in Figure 1A. Data are plotted as a function of drug molecules bound per duplex, as calculated from a comparison of changes in refractive index caused by ACTD binding and DNA hybridization.[30] Data are corrected with a poly(dT) background and scaled to account for the contribution of drug binding to ssDNA. Lines are fits for k_{obs} to the data using the simplified Langmuir equation (eq 1). All ACTD binding was carried out in 0.1 M NaCl/TE and monitored at 56.0°.

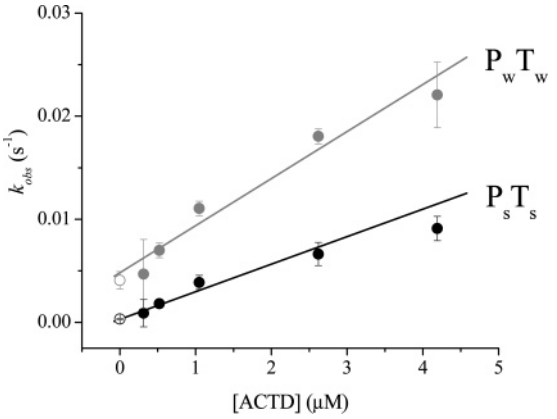

Figure 4. Plot of k_{obs} values (solid points), obtained from fitting of adsorption curves in Figure 3, as a function of ACTD concentration for each duplex. The solid lines are weighted linear fits to the average k_{obs} values and their associated errors. The error bars represent both fitting errors and spot-to-spot variation. At high concentrations, reaction rates are more rapid, and rate constants k_{obs} obtained from fitting the onset of binding have higher associated error. At very low concentrations, errors are high because of low signal-to-noise for the small signal levels and possible approach to a break-down of pseudo-first-order kinetics. The slope of each line represents the drug association rate constant for each duplex (k_a = (2.67 ± 0.08) × 10^3 M^{-1} s^{-1} for P_sT_s and (4.57 ± 0.20) × 10^3 M^{-1} s^{-1} for P_wT_w). The *y*-intercepts indicate the drug dissociation rate constant for each duplex (k_d^{-1} = 3300 ± 100 s for P_sT_s and 210 ± 15 s for P_wT_w). Open circles at the *y*-intercept were determined independently from fitting desorption data, Figure 5, to eq 2. These points were not included in the determination of best-fit line but are in excellent agreement.

where k_{obs} is the observed association rate ($k_{obs} = k_aC + k_d$), $\%\Delta R(t)$ is the time-dependent change observed in reflectance upon injection of a particular ACTD concentration (C), and f_{max} is the reflectance change obtained when a fraction of binding sites are occupied by the drug. k_a and k_d are the true drug association and dissociation rate constants. The resultant k_{obs} values were plotted against concentration, as shown in Figure 4, and the slope of k_{obs} vs [ACTD] was used to obtain the true surface drug association rate constant for each duplex. These values of k_a, (2.67 ± 0.08) × 10^3 and (4.57 ± 0.20) × 10^3 M^{-1} s^{-1} for P_sT_s and P_wT_w, respectively, agree generally with a surface association rate constant of (6 ± 1) × 10^3 M^{-1} s^{-1} measured by reflectometric interference spectroscopy for ACTD binding to physisorbed biological DNA.[41]

Although there is some apparent curvature at the highest concentrations studied, there are also large errors. Our analysis is based on a linear fit, which is the simplest model that is generally consistent with the data within error, rather than a complex model with more parameters that could account for curvature. Indeed, curvature in Figure 4 may have several possible explanations. One explanation is that the mechanism of reaction deviates from the single-step non-cooperative association/dissociation model invoked here. For example, a two-step model often referred to as an "induced fit" model could show negative curvature. We believe this explanation is unlikely, since solution experiments show no evidence of such cooperativity. A second explanation is that the curvature is due to reduction of the activity of ACTD at high concentrations and that this effect is more pronounced for binding events at the interfacial architecture of these monolayer films compared with behavior in bulk solution. Finally, the tendency of ACTD to form relatively stable aggregates in aqueous solution may also play a part. A rough estimate, based on NMR studies in deuterated water,[42] is that ~2% of the ACTD is in dimer form at the highest concentration.

In contrast with adsorption, the drug desorption rates measured for the two duplexes differ by more than an order of magnitude. ACTD desorbs very slowly from the binding sites of P_sT_s (k_d^{-1} = 3300 ± 100 s) and relatively quickly from the binding sites of P_wT_w (k_d^{-1} = 210 ± 15 s). These values were obtained from the *y*-intercepts of the slopes of the linear fits in Figure 4 ($k_{obs} = k_aC + k_d$).

These results are further confirmed by analyzing the measured desorption curves (Figure 5) with a single-exponential decay model:

$$\%\Delta R(t) = f_{max}\, e^{-(k_d)t} \qquad (2)$$

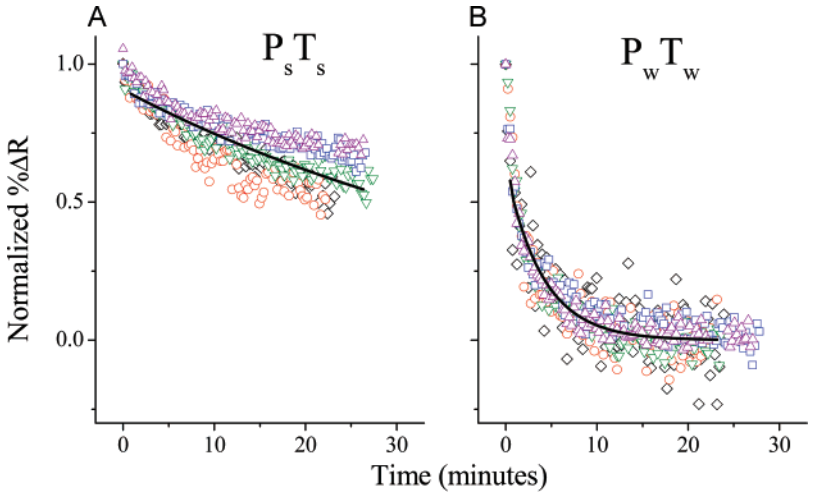

Figure 5. Normalized ACTD dissociation from DNA duplex films, P_sT_s (A) and P_wT_w (B), on the same patterned surface after binding at various concentrations. Symbols indicating concentration are the same as in Figure 3. Dissociation is initiated by replacing the ACTD solution with 0.1 M NaCl/TE buffer starting at $t = 0$. The solid lines are single-exponential fits to the averaged data (averaged for all concentrations). The dissociation rate constants obtained from both fits ($k_d^{-1} = 3100 \pm 700$ s for P_sT_s and $k_d^{-1} = 250 \pm 50$ s for P_wT_w) agree very well with the values independently obtained from association rate analysis. Note: For analysis of P_sT_s data, it was necessary to force the final fit value to zero since ACTD does not completely desorb from the surface on the experimental time scale. For all data, the first 30 s were not included in the fit because of the uncertainty in these points caused by rinsing buffer through the liquid cell. P_wT_w dissociation data were corrected for DNA target loss during buffer exposure, as discussed in the Supporting Information (Figure S7).

Table 2. Summary of Kinetic and Thermodynamic Constants for ACTD Binding

	25-mer, three binding sites							10-mer, one binding site solution	
	surface			solution					
	k_a (M^{-1} s^{-1}) $\times 10^3$	k_d^{-1} (s)	K_A (M^{-1})[a] $\times 10^6$	k_a (M^{-1} s^{-1}) $\times 10^5$	$k_{d,SDS}^{-1}$ (s)	k_d^{-1} (s)[b]	K_A (M^{-1}) $\times 10^6$	$k_{d,SDS}^{-1}$ (s)[c]	K_A (M^{-1})[d] $\times 10^6$
P_sT_s (TGCT)	2.67 ± 0.08	3300 ± 100	8.8	3.9 ± 0.7	1400 ± 200	105	41 ± 23	730	6.7
P_wT_w (GGCA)	4.57 ± 0.20	210 ± 15	1.0	4.9 ± 0.5	82 ± 4	9.0	4.4 ± 0.8	~60	2.1

[a] Calculated from measured surface association and dissociation rate constants. [b] Calculated from the measured solution association rate constant and binding affinity. [c] From Chen,[11] determined from 1% SDS-induced dissociation kinetics monitored at 452 nm. [d] From Chen,[11] measured by solution-phase titration (not kinetics) in 0.1 M NaCl/Tris-HCl.

The desorption rate in this physical model is independent of drug concentration. The averages of normalized desorption curves for all concentrations are fit to eq 2 to obtain drug dissociation rates for each film. Within error, these values ($k_d^{-1} = 3100 \pm 700$ and 250 ± 50 s for P_sT_s and P_wT_w films, respectively) agree with those extrapolated from plots of k_{obs} vs [ACTD] and are plotted in Figure 4 as open symbols at [ACTD] = 0 μM. Although absolute values cannot be compared directly with solution-phase rates measured from shorter, less stable strands by SDS-induced dissociation, it is interesting that the *ratio* of the dissociation rate constants for the binding sites (TGCT:GGCA) measured on the surface agrees well with solution measurements reported by Chen.[11]

We note that the dissociation data in Figure 5B for P_wT_w films are, as expected, independent of drug concentration, but the data from P_sT_s films (Figure 5A) appear to deviate. Dissociation at lower concentration appears to proceed slightly more rapidly. In principle, this could arise from cooperativity in ACTD dissociation; however, that is not the case here. Rather, the reason for the deviation is that the data in Figure 5A are un-corrected for concentration-dependent target DNA loss, which is largest at low concentrations. Very little target DNA loss occurs during rinsing of highly loaded DNA-drug complexes because of maximized duplex stability. For P_sT_s at 4 μM [ACTD], there are almost three drug molecules per duplex, compared with one per duplex at 0.3 μM [ACTD] (Figure 3A). If ACTD dissociation is complete during the buffer exposure time, it is straightforward to correct for this phenomenon (as was done for the data in Figure 5B, see Figure S7); however, the slow dissociation data in Figure 5A could not be corrected without introducing possible bias. Thus, the dissociation rate constant obtained from the average in Figure 5B for the P_sT_s sequence is probably somewhat of an overestimate.

While the k_d values for the binding sites studied differ by an order of magnitude, the k_a values are more similar, differing by less than a factor of 2. The lack of strong binding-site dependence on ACTD association rates measured on the surface is consistent with initial nonspecific binding of drug to duplex. This observation is supported by time-dependent DNAse I footprinting studies, showing that ACTD interacts with the DNA duplex initially through non-sequence-specific minor groove sites and then "shuffles" along the DNA until intercalating at its preferred binding site.[43] The dissociation rate, which is strongly sequence-specific, contributes more strongly to the drug binding affinity.

We determine the surface binding affinities for each duplex using our measured kinetic rate constants ($K_A = k_a/k_d$). These values, listed in Table 2, indicate that ACTD binds more strongly to the sites in P_sT_s ($K_A = 8.8 \times 10^6$ M^{-1}) than P_wT_w ($K_A =$

(41) Piehler, J.; Brecht, A.; Gauglitz, G.; Zerlin, M.; Maul, C.; Thiericke, R.; Grabley, S. *Anal. Biochem.* **1997**, *249*, 94−102.
(42) Angerman, N. S.; Victor, T. A.; Bell, C. L.; Danyluk, S. S. *Biochemistry* **1972**, *11*, 2402−2411.
(43) Bailly, C.; Graves, D. E.; Ridge, G.; Waring, M. J. *Biochemistry* **1994**, *33*, 8736−8745.

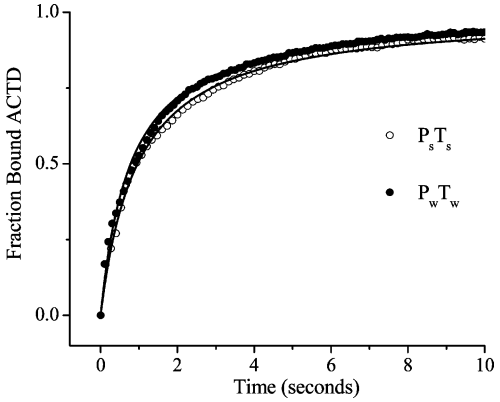

Figure 6. Solution-phase kinetic measurements of ACTD binding to duplexes P_sT_s and P_wT_w. Equimolar (5 μM) solutions of ACTD and each duplex were mixed together at $t = 0$ by syringe injection into an empty cuvette (final solution volume and concentration, 0.3 mL and 2.5 μM). Absorbance changes at 427 nm were monitored at 20 °C for two trials of each sequence. Although absorbance decreases at this wavelength upon drug binding, the data are plotted in terms of ACTD fraction bound. Data are fit to eq 3 (solid lines), and similar values of k_a are extracted for each duplex (see Table 2). This plot represents the average of two trials for each sequence. Errors in the obtained association rate constants represent trial-to-trial variation. All experiments were carried out in 0.1 M NaCl/TE.

1.0×10^6 M^{-1}) on the surface. These K_A values agree with those measured by titration for short strands in solution (also listed in Table 2),[11] demonstrating that SPR imaging can discriminate between drug binding sites in addition to simultaneously providing mechanistic information about the DNA−drug interaction. However, to further demonstrate the feasibility of SPR imaging as a drug screening technique, we assess the effect the surface has on such biosensor measurements. It is well-known that surface interactions can be hindered by conformational restriction of probe molecules. For example, it has been shown for DNA hybridization that associative surface binding constants are generally smaller than those in solution.[44] We[37] and others[45] have also shown that the surface suppresses DNA hybridization rates compared to those in solution. One study of small-molecule binding to dextran-immobilized protein, however, found rate and affinity constants that closely match those measured in solution.[46] However, no direct solution/surface comparison has been made for DNA−drug interactions. Therefore, we measure specific rate and affinity constants for our P_sT_s and P_wT_w probe duplexes in solution.

Solution-Phase Kinetic and Thermodynamic Comparison. We find similar association rates for the two binding sites studied in solution ($(3.9 \pm 0.7) \times 10^5$ and $(4.9 \pm 0.5) \times 10^5$ M^{-1} s^{-1} for P_sT_s and P_wT_w, respectively). Surface association rates for the two binding sites were also identical within a factor of 2 (column 4, Table 2). Figure 6 displays the solution-phase kinetics of ACTD binding to equimolar concentrations of P_sT_s and P_wT_w. Drug association was monitored at 427 nm by absorption spectroscopy after injection of drug and duplex into an empty cuvette. The change in absorbance measured upon drug binding over time (A_t) can be described by second-order kinetics:

$$A_t = A_o + (A_\infty - A_o)\frac{C_o k_a t}{1 + C_o k_a t} \quad (3)$$

where A_∞ is the absorbance of bound drug at equilibrium, A_o is the initial absorbance of free drug, and C_o is the initial (equal) concentration of both drug and duplex. Fits to this equation yield solution-phase drug association rate constants. Dissociation rates are not considered in this analysis because, under the conditions used, $k_a \gg k_d$.

The solution-phase rate constants are each approximately 100-fold faster than those obtained from surface binding; binding occurs in seconds rather than minutes, as measured by SPR imaging. Surface suppressions have also been observed for the rates of DNA−DNA hybridization on both microparticles and planar surfaces compared to those observed in solution.[37,45] Mass transport in bulk solution cannot be responsible for the suppression observed here and in these previous DNA hybridization studies; experimental conditions (large cell volume, micromolar concentrations) rule out transport-limited kinetics. Because ACTD is also a neutral species under these experimental conditions, electrostatic hindrance cannot be responsible for the suppression, as is sometimes the case for DNA hybridization.[47] Rather, the suppression is most likely caused by steric hindrance and/or large entropic penalties associated with DNA−drug complexation at the surface.

We also find a higher ACTD binding affinity for both P_sT_s and P_wT_w in solution. Figure 7 shows the spectral titration results for adding increasing amounts of duplex DNA to a fixed concentration of ACTD in solution. The observed changes in absorbance at 440 nm ($\Delta A_{440\ nm}$) vs [DNA] were fit using a two-state model and considering the number of drug binding sites per duplex, n:

$$K_A = \frac{Y}{(n[\mathrm{DNA}] - Y)([\mathrm{ACTD}] - Y)} \quad (4)$$

where [DNA] and [ACTD] are the total concentrations of duplex and drug in solution, respectively. The parameter Y represents the concentration of bound drug and is equal to $\Delta A_{440nm}/\Delta\epsilon_{440nm}$, where $\Delta\epsilon_{440nm}$ is the difference in molar extinction coefficients for free and bound ACTD determined experimentally for each duplex. For P_sT_s and P_wT_w, we measured $\Delta\epsilon_{440nm} = 9500$ and 8500 M^{-1} cm^{-1}, respectively.

Fitting to eq 4 revealed binding affinities approximately 4 times higher in solution than on the surface (see Table 2 for values). Data fitting also yielded values of n (binding sites per duplex) of 4.5 and 5.2 for P_wT_w and P_sT_s, respectively. These high n values are most likely caused by nonspecific drug−duplex binding or drug aggregation[42] at the higher concentrations ($\sim$7 μM) necessary for titration.

Using $k_d^{-1} = K_A/k_a$, we calculate values of $k_d^{-1} = 105$ s for P_sT_s and 9.0 s for P_wT_w. Comparing these values to those measured on the surface, we find a 25-fold surface suppression. Because dissociation measurements in solution are typically carried out in SDS, we also did a similar experiment for direct comparison and found SDS-induced desorption rates to be generally 10 times slower than true rates in solution. Induced rates are displayed in Table 2 (see Supporting Information, Figure S8, for measurement details).

(44) Levicky, R.; Horgan, A. *Trends Biotechnol.* **2005**, *23*, 143−149.
(45) Henry, M. R.; Stevens, P. W.; Sun, J.; Kelso, D. M. *Anal. Biochem.* **1999**, *276*, 204−214.
(46) Day, Y. S. N.; Baird, C. L.; Rich, R. L.; Myszka, D. G. *Protein Sci.* **2002**, *11*, 1017−1025.
(47) Vainrub, A.; Pettitt, B. M. *Biopolymers* **2003**, *68*, 265−270.

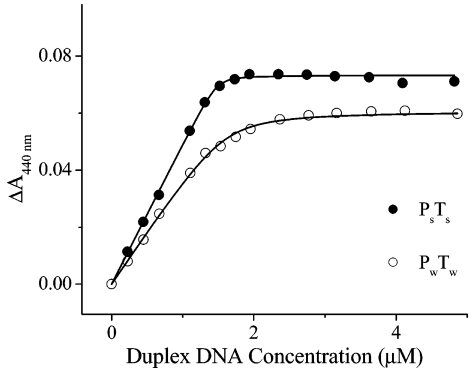

Figure 7. Solution-phase reverse spectral titration results for P_sT_s and P_wT_w added to a solution of ACTD (fixed at ~7 μM in 0.1 M NaCl/TE). Data were corrected for dilution and fit to eq 4. Values of K_A were found to be $(41 \pm 23) \times 10^6$ and $(4.4 \pm 0.8) \times 10^6$ M^{-1} for P_sT_s and P_wT_w, respectively. Errors in the binding affinities come from data fitting.

Overall solution/surface differences seem to derive mostly from the ACTD association rates, suggesting the existence of a larger barrier to drug surface adsorption than surface desorption. This barrier may be steric; ACTD might need to penetrate into the brush-like DNA film in order to bind to buried sites. However, the barrier may also be entropic in nature. It is known that solution-phase DNA−drug intercalation is enthalpically driven but also entropically costly.[48] On the surface, enthalpy changes associated with DNA−drug intercalation may be similar to those in solution, but entropic penalties due to loss of translational/rotational freedom and damped motion of the DNA duplex could be enhanced for the immobilized complex.

Conclusions

We have shown that, with appropriate control experiments and careful data analysis, array-based SPR imaging can be used to measure the kinetics and thermodynamics of sequence-dependent DNA−drug binding. For the first time, we are able to discriminate between different drug binding sites on the same DNA-based sensor surface with a refractive-index-based detection technique. With angle-resolved imaging, we directly determine the number of drug molecules bound to each type of surface-immobilized DNA, detecting down to less than one drug molecule per duplex. We are also able to compare kinetic and affinity constants obtained by SPR imaging to measured solution-phase values in order to determine surface effects on DNA−drug interactions. Binding affinity is suppressed ~4-fold by the sensor surface, mainly due to a barrier to drug adsorption; association rates are ~100 times faster in solution than on the surface. Using only a few array probe spots, we have demonstrated the utility of SPR imaging as a screening method in drug discovery. High-throughput determination of binding mechanisms and kinetics for a large number of drug candidates and binding sites using this method would require only a scale-up of spot patterning and fluid handling.

Acknowledgment. This work was supported in part by the National Science Foundation (DBI-0096731) and by the National Cancer Institute of the National Institutes of Health (CA 89562).

Supporting Information Available: Control studies for nonspecific ACTD binding and DNA target cross-hybridization to array surfaces; studies determining ACTD non-cooperativity for three binding-site duplexes used in this work; demonstrations of ACTD kinetic adsorption and desorption data corrections (background selection, ssDNA−ACTD binding, and dissociation of DNA target from surface during rinsing). This material is available free of charge via the Internet at http://pubs.acs.org.

JA072401L

(48) Chaires, J. B. *Arch. Biochem. Biophys.* **2006**, *453*, 26−31.